https://doi.org/10.5194/ar-2026-14
Preprint. Discussion started: 5 May 2026
© Author(s) 2026. CC BY 4.0 License.

AEROSOL Research Discussions

Co-condensation and co-evaporation of levoglucosan onto and from deliquesced ammonium sulfate particles – influence of relative humidity, particle mass and size, and presence of a surfactant

Jian Xu[1, a, *], Junteng Wu[1,2,*], Mayur Gajanan Sapkal[3], Jim Grisillon[1], Shravan Deshmukh[4], Brice Temime Roussel[1], Julien Kammer[1], Nicolas Brun[1], Fabien Robert-Peillard[1], Beiping Luo[3], Judith Kleinheins[3], Silvia Henning[4], Bénédicte Picquet-Varrault[5], Edouard Pangui[5], Mathieu Cazaunau[5], Zamin A. Kanji [3], Claudia Marcolli[3], Anne Monod[1]

[1]Aix Marseille Université, CNRS, LCE, Marseille, France

[2]Université Clermont Auvergne, CNRS, OPGC, LaMP, F-63000 Clermont Ferrand, France

[3]Institute for Atmospheric and Climate Science, ETH Zürich, Zürich, Switzerland

[4]Leibniz Institute for Tropospheric Research (TROPOS), 04318 Leipzig, Germany

[5]Univ Paris Est Creteil and Université de Paris Cité, CNRS, LISA, F-94010 Créteil, France

[a]Now at Department of Chemistry, University of Oslo, Oslo, Norway.

* Two first authors, as both authors contributed equally to this work

Correspondence to: Jian Xu (jianxuu@gmail.com), Junteng Wu (junteng.wu@uca.fr) and Anne Monod (anne.monod@univ-amu.fr)

Abstract

Co-condensation is the process by which condensable vapors condense alongside water vapor onto growing aerosols, and it can significantly alter the properties of clouds. Semi-volatile species partition dynamically between the gas and the condensed phases, and their co-condensation together with water vapor may increase the condensed mass and amplify water uptake. Although this process is based on thermodynamics and has been simulated in models, it has been scarcely investigated experimentally. In this study, the ability of levoglucosan to co-condense and co-evaporate from inorganic particles together with water was investigated by monitoring, under ambient-like conditions, its gas-particle partitioning on ammonium sulfate (AS) monodispersed particles in the Experimental Multiphasic Atmospheric Simulation Chamber (CESAM). The net evaporation flux of levoglucosan depending on particle size and the presence of a surfactant was explored for relative humidities (RH) from 100% to dry conditions as particle concentration in the chamber was reduced. Due to the high deliquescence point of AS, wet experiments were initialized at RH above 80%. Co-condensation of levoglucosan was observed when RH increased up to 100%, while co-evaporation of levoglucosan occurred when RH decreased. It was shown that gas-particle partitioning of levoglucosan was sensitive to all the investigated parameters, but the main drivers were the levoglucosan-to-sulfate mass ratios and RH. The effect of the levoglucosan-to-sulfate mass ratio was interpreted as salting-out, and the significant influence of RH provides experimental proof of co-evaporation or co-condensation of levoglucosan from or onto AS particles.

https://doi.org/10.5194/ar-2026-14
Preprint. Discussion started: 5 May 2026
© Author(s) 2026. CC BY 4.0 License.

AEROSOL Research Discussions

1. Introduction

Co-condensation is the process by which condensable vapors condense alongside water vapor onto growing aerosols (Kulmala et al., 1993;Topping et al., 2013). This can significantly alter the properties of clouds (Kulmala et al., 1997). Indeed, the co-condensation of gas-phase semi-volatile organic substances together with water vapor may increase the condensed mass and amplify water uptake. Semi-volatile species partition dynamically between the gas and the condensed phases (Ijaz et al., 2025;Thompson et al., 2017;Lopez et al., 2025;Donahue et al., 2006). As relative humidity (RH) increases, water condenses on particles, increasing the condensed volume and enhancing the condensation of semi-volatile species. Conversely, when RH decreases, water evaporates from the particles, along with semi-volatile species. Although this process is based on thermodynamics and has been simulated in models, few studies have investigated it experimentally. Several field studies coupled to models have shown that this effect is potentially large for secondary organic aerosol (SOA) containing a large fraction of semi-volatile species (Wang et al., 2025;Heikkinen et al., 2024;Rastak et al., 2017;Topping et al., 2013;Topping and McFiggans, 2012;Topping et al., 2011). In the same way, a new "diagonal" volatility basis set has been developed to assess the condensation of organic vapors onto particles and was tested in several CLOUD chamber experiments on α-pinene SOA (Lopez et al., 2025). However, this process has never been experimentally investigated on a single semi-volatile compound under various controlled conditions.

In the present study, we have investigated experimentally the ability of a single semi-volatile organic compound to co-condense and co-evaporate from inorganic particles under various conditions. Levoglucosan (1,6-anhydro-β-D-glucopyranose, $C_6H_{10}O_5$) was chosen because it is a semi-volatile compound (Zhang et al., 2024) that is miscible with water. The molecule bears 3 hydroxyl groups that can provide strong H-bonds with water molecules and ions (Qin et al., 2021;Pye et al., 2018). Furthermore, levoglucosan is a widely used molecular marker of biomass burning in the atmosphere, it has high emission factors and is almost exclusively emitted by the pyrolysis of cellulose and hemicellulose. It has been measured in particles at various sites all over the world, and overall, 90% of levoglucosan mass concentrations were found in particles with aerodynamic diameters of less than 2 µm (Bhattarai et al., 2019). However, levoglucosan is semi-volatile and water-soluble. Consequently, its mass fraction in particles is influenced by long-range transport, as well as by particle-phase mixing, evaporation, co-condensation, and multiphase chemical (and biological) processes (Bhattarai et al., 2019;Yazdani et al., 2023).

To investigate the ability of a semi-volatile water-soluble organic compound to co-condense and co-evaporate from inorganic particles, the gas-particle partitioning of levoglucosan was monitored under ambient-like concentrations on ammonium sulfate (AS) monodispersed particles in the CESAM simulation chamber (French acronym for Experimental Multiphasic Atmospheric Simulation Chamber). Various conditions were explored, including relative humidity (from dry to 100% RH), dilution, particle mass and size, and the presence of a surfactant on the particles. The net evaporation flux of levoglucosan was quantified under each condition.

2. Methods

To investigate the partitioning behavior of levoglucosan onto AS particles under dry and high RH conditions, fifteen experiments were performed under controlled conditions, as shown in Table

https://doi.org/10.5194/ar-2026-14
Preprint. Discussion started: 5 May 2026
© Author(s) 2026. CC BY 4.0 License.

1. Except for those performed under dry conditions, all the experiments were started at RH above the deliquescence point of AS particles. This was done to focus the study on the effects of levoglucosan (partitioning into an aqueous AS particle) on particle growth or shrinking as a function of RH.

Two control experiments (1a, 1b) were performed under high RH without levoglucosan, using AS particles of two different selected dry sizes (electrical mobility diameters of ~100 and ~200 nm, respectively). Note that OA contributed to 10 and 8% of the total particle mass for Exp 1a and 1b, respectively, in good agreement with (Wu et al., 2022).

The partitioning of levoglucosan onto AS particles was investigated under constant RH conditions: three experiments under dry conditions (exp. 2a, 2b, 2c with selected electrical mobility diameters of ~200, ~200 and ~100 nm, respectively) and three under constant high RH conditions (exp. 3a, 3b, 3c with selected dry electrical mobility diameters of ~100, ~100 and ~200 nm).

The impact of varying RH on levoglucosan partitioning was examined in three experiments with a selected dry electrical mobility diameter of ~200 nm (exp. 3d, 3e, 3f), and in two experiments with a selected dry electrical mobility diameter of ~100 nm (exp. 3g, 3h).

Finally, two experiments (4a, 4b) were conducted to investigate the effect of a surfactant on levoglucosan partitioning. These two experiments were conducted under the same conditions as experiments 3f and 3c, respectively, but sodium dodecyl sulfate (SDS) was added to the solution to generate particles. SDS was chosen as one of the most well-characterized water-soluble surfactants. It is also slightly soluble in AS aqueous solutions, which were nebulized under the same conditions as in all the other experiments (Faust and Abbatt, 2019).

Table 1. Summary of the experimental conditions. NA = non available; k_{net} is the net evaporation rate of organic matter from AS particles. All numbers, except for T and k_{net} are given at time 0, when the introduction of particles stopped. T are the temperature average values, and the k_{net} values are determined from the exponential fitting of the time profiles of organic-to-sulfate mass ratio $f_{o/s}$ (see Sect. 2.6).

Exp no.	Aerosol type	T (°C) ±0.1	RH (%) ±0.8	[number] (10^4 #/cm^3) ±5%	D_{ve} dry* (nm) ± 7 %	[mass]* (µg.m^{-3}) ± 26%	OA/sulfate ($f_{o/s}$)	k_{net} (× 10^{-5} s^{-1})	Exp. date yy/mm/dd
1a	AS	24.0	89.4	2.33	90.1	15.7	0.14± 0.01	NA	24/03/18
1b	AS	24.1	94.1	1.35	146	38.6	0.091± 0.001	NA	24/03/19
2a	AS/Levo	21.9	0	1.01	164	32.6	1.79± 0.01	1.66 ± 0.01	24/03/01
2b	AS/Levo	21.7	0	1.09	174	38.8	2.10± 0.01	1.64 ± 0.02	24/03/04
2c	AS/Levo	23.0	0	4.37	98.7	23.8	1.66± 0.01	5.41 ± 0.05	24/03/05
3a	AS/Levo	22.4	88.7	1.89	NA	NA	2.29± 0.02	6.00 ± 0.09	24/03/06
3b	AS/Levo	22.4	88.1	3.55	93.7	18.8	2.13± 0.02	4.36 ± 0.06	24/03/07
3c	AS/Levo	22.4	85.5	0.969	174	32.3	2.33± 0.01	3.36 ± 0.05	24/03/08
3d	AS/Levo	23.1	97.8	0.715	166	29.7	2.08± 0.01	-1.15 ± 0.10	24/03/11
		23.2	99.8	0.446	169	19.4	2.13± 0.02	0.91± 0.09	
		23.4	96.0	0.331	169	14.6	1.99± 0.02	4.44 ± 0.14	
3e	AS/Levo	23.8	86.0	1.02	175	49.8	2.38± 0.01	3.26 ± 0.06	24/03/12
		23.7	76.0	0.664	160	24.7	1.76± 0.03	11.5± 0.3	
3f	AS/Levo	24.4	85.1	0.918	177	45.4	2.39± 0.01	4.21 ± 0.07	24/03/13
		24.5	90.0	0.605	174	28.6	1.88± 0.02	11.6 ± 0.2	
		24.8	65.1	0.405	159	14.8	0.82± 0.02	29.3 ± 0.8	
3g	AS/Levo	23.8	85.7	1.77	93.9	13.7	1.54± 0.02	15.9 ± 0.3	24/03/14

https://doi.org/10.5194/ar-2026-14
Preprint. Discussion started: 5 May 2026
© Author(s) 2026. CC BY 4.0 License.

3h	AS/Levo	24.4 24.5	89.2 90.1	2.92 1.73	79.8 78.0	13.3 7.2	2.25± 0.04 1.11± 0.03	14.2 ± 0.3 29.3 ± 1.0	24/03/15
4a	AS/Lev/SDS	24.5 24.7	88.5 87.2	NA 0.742	NA 186	NA 37.6	3.45± 0.02 3.30± 0.03	6.34 ± 0.18 14.7 ± 0.6	24/03/20
4b	AS/Lev/SDS	25.6	84.8	0.879	180	41.6	3.28± 0.02	9.14 ± 0.33	24/03/21

* Corrected data (see Sect. 2.5.2)

2.1 CESAM chamber and experimental design

The CESAM chamber has been used extensively in recent years for the study of atmospheric multiphase processes and is described in detail in Wang et al (Wang et al., 2011). The chamber is made of stainless steel, with a volume of 4.2 m^3 and a surface-to-volume ratio of 4.3 m^{-1}. Purified humidified (or dry) air inlet flow is employed to offset sampling flows and maintain automatically the requested pressure. A mixing time of approximately one minute within the chamber is ensured by a 50 cm diameter stainless steel fan. The chamber is equipped with a wide range of analytical instruments to measure physical parameters such as pressure (Baratron MKS), temperature (Type T Thermocouple - 321 Stainless Steel Sheath (400°C), TC-Direct), RH (Chilled Mirror, Michell Optidew model 501). Special care was taken with RH control and measurements, particularly for experiments performed at high RH. The saturation water vapor pressure was derived from the dew point measured by the chilled mirror using the Buck equation (Buck, 1981), and the water vapor pressure was derived from the same equation, but using the average temperature provided by three thermocouples T sensors suspended in the air inside CESAM. RH was calculated as the ratio between these two vapor pressures.

The chamber also provides additional connections for other dedicated instruments that were required (described in Sect. 2.5). All these instruments were operated online, leading to a constant air flow out of the chamber, which was continuously compensated by an inflow of humid N_2, inducing continuous dilution of the mixture inside the chamber. The humidification of N_2 was done using the HUMANS set up (described in Sect. 2.2), which allowed a precise control of RH throughout each experiment. To minimize contamination from external air, the chamber was operated at a pressure of 5 mbar above the prevailing ambient one. In addition, the chamber was daily vacuumed after each experiment and remained under vacuum (i.e. 1×10^{-3} mbar) overnight with its walls heated at 55 °C, and the inner walls of the chamber were manually cleaned prior to each new series of experiments.

2.2 HUMidificAtioN System (HUMANS) to regulate the relative humidity at high values in the chamber

At the start of each experiment, a known quantity of water (92 g on average) was introduced into CESAM under vacuum, and then dry nitrogen was added to reach the desired pressure (5 mbar above ambient). The amount of water introduced was calculated to achieve a relative humidity (RH) of ~90% when the desired pressure was reached. Because RH was difficult to maintain at high RH, the HUMidificAtioN System (HUMANS) was then connected to CESAM to regulate RH precisely by adjusting the RH of the nitrogen input, which had an initial RH of less than 10%. The HUMANS system was employed to precisely maintain or decrease the desired RH within CESAM throughout

https://doi.org/10.5194/ar-2026-14
Preprint. Discussion started: 5 May 2026
© Author(s) 2026. CC BY 4.0 License.

the experimental period. HUMANS can generate a total flow of up to 40 L min^{-1}, but was operated at a constant total flow rate of 10 L min^{-1} in this study. It utilizes two mass flow controllers (MFCs; Alicat MC-20SLPM), referred to as MFC1 and MFC2 (see Fig. 1). The dry N_2 flow through MFC1 is routed through four Nafion humidifiers (Perma Pure MH-110) connected in series (as shown in Fig. 1). These tubes are surrounded by Milli-Q water, which is circulated via a thermostatically controlled water bath (Lauda E306) maintained at ~25 °C. Water vapor diffuses through the Nafion membranes, producing a humidified N_2 stream (sky blue colour line in Fig. 1). Simultaneously, a separate dry N_2 stream from MFC2 bypasses the Nafion tubes. The humidified and dry streams are mixed downstream, enabling precise RH control through dynamic adjustment of the individual MFC flow rates.

The final RH of the flow was typically set to match the target RH of the chamber. To do so, the CESAM compensating flow (which is ≥ 10 L min^{-1}) was divided into two: i) a constant 10 L min^{-1} flow passed through HUMANS, and ii) the rest of the passed through a heated water bubbler. For instance, to maintain a chamber RH of 65%, 6.5 L min^{-1} was directed through MFC1 and 3.5 L min^{-1} through MFC2. For near-saturation conditions (~90% RH), the full 10 L min^{-1} flew through MFC1, while for dry conditions (<30%), MFC1 was shut off and only dry N_2 from MFC2 was supplied to the chamber. The final RH of the mixed flow was monitored in real time using a calibrated temperature and humidity sensor (Sensirion SHT75). Sensor feedback was integrated into a Python-based control interface, which dynamically adjusted the flow rates to maintain the target RH with high accuracy and stability. To prevent contamination and ensure reproducibility, the Milli-Q water used in the humidification bath was replaced daily prior each experimental run.

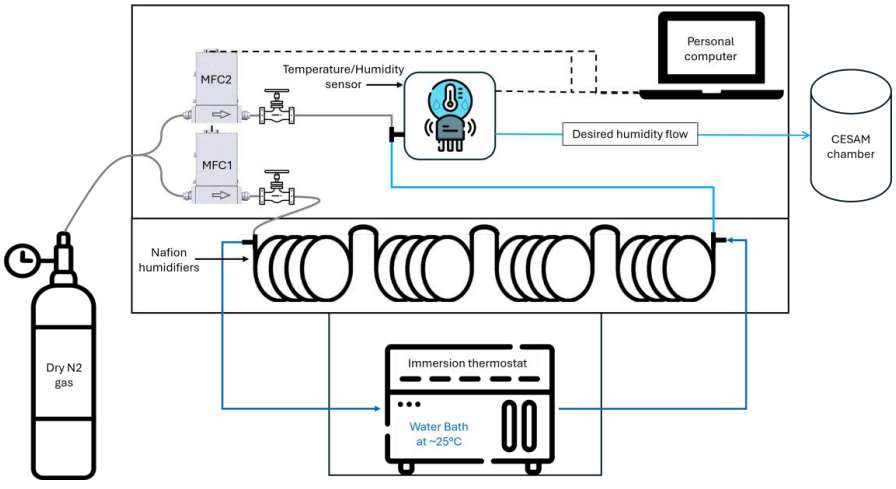

Figure 1. Schematic of HUMANS (HUMidificAtioN System) for regulating relative humidity (RH) within the CESAM chamber. MFC1 and MFC2 represent the mass flow controllers, where MFC1 directs dry nitrogen through the Nafion humidifiers, while MFC2 controls the dry nitrogen flow for mixing. The dark blue line indicates the circulating water from the thermostatically controlled water bath. The grey and light blue lines represent the dry nitrogen stream (RH <10%) and the humidified nitrogen stream, respectively. The dashed black line denotes the system components monitoring and control via the computer interface.

https://doi.org/10.5194/ar-2026-14
Preprint. Discussion started: 5 May 2026
© Author(s) 2026. CC BY 4.0 License.

2.3 Chemical reagents

Levoglucosan (purity: 99%), ammonium sulfate (99.9999% Suprapur) and sodium dodecyl sulfate (SDS; purity: ≥99.0%) were purchased from Sigma-Aldrich. LC-MS grade water (Thermo Fisher Scientific Inc.) has been used for preparing the solutions to be nebulized in the chamber and for maintaining the desired RH in the tank. The particles were generated by nebulization of 50 mL solutions containing 15 g L^{-1} of AS and 15 g L^{-1} of levoglucosan, freshly prepared on the day of each experiment. For SDS experiments, the solution composition was 15 g L^{-1} of AS, 15 g L^{-1} of levoglucosan and 4.6 g L^{-1} of SDS. The latter concentration was chosen after pre-experiments of nebulization using AS + SDS, which confirmed the feasibility of nebulizing SDS + AS solutions to generate monodispersed particles of the desired diameter, and the necessity of using a large impactor between the atomizer and the Nafion dryer (see Supplementary Information SI-1).

2.4 Introduction of monodisperse particles

An atomizer (TSI Model 3076) was used to produce polydisperse aerosols. The particles then passed through a dryer and an Aerodynamic Aerosol Classifier (AAC, Cambustion). In the AAC, the particle aerodynamic diameters were selected at 170 or 300 nm, corresponding to particle mobility diameters of approximately 100 or 200 nm, respectively. The conversion from aerodynamic to mobility diameter was further confirmed using the shape factor and the mixed density, using the AMS data (DeCarlo et al., 2004). Before introducing the particles into CESAM, the size-selection performance of the AAC was verified by measuring the monodisperse size distribution using a TSI SMPS placed at the AAC outlet. Once this monodisperse size distribution was Gaussian, aerosols from the AAC outlet were introduced into the chamber. The aerosol flow rate through the AAC and into the chamber was maintained within 1-2 L min^{-1}, with aerosol concentrations of approximately 4×10^5 particles cm^{-3} for 100 nm and 3×10^5 particles cm^{-3} for 200 nm, respectively. One to two hours of injection were required to achieve target number concentrations of at least 10 000 particles cm^{-3} of 100 nm and 8000 particles cm^{-3} of 200 nm particles in CESAM. These values were targeted to ensure sufficient particles to be detected after several hours of experiment while avoiding coagulation. At the same time, a flow of humid nitrogen was introduced into the chamber to adjust the relative humidity, which was controlled by the HUMANS system.

2.5 Particle characterization in CESAM

2.5.1 Characterization of chemical composition of particles

The chemical composition of particles was measured with the Aerodyne high-resolution time-of-flight aerosol mass spectrometer (AMS) (Drewnick et al., 2005;DeCarlo et al., 2006). Standard calibrations were performed using 300 nm size-selected dried ammonium nitrate and ammonium sulfate particles at the beginning and the end of the campaign. The data were analyzed using the ToF-AMS HR Analysis Toolkit v1.25, which includes Pika version 1.25F and Squirrel version 1.65F. To verify that the organic signal detected by the AMS corresponds to levoglucosan, we used the characteristic levoglucosan marker m/z 60.02, as described in previous studies (Lee et al., 2010;Alfarra et al., 2007), corresponding to the fragment $C_2H_4O_2$ in HR MS. The contribution of the signal at m/z 60.02 to the total organic aerosol signal remained constant throughout each experiment. In experiments 4a and 4b, involving the addition of SDS, we used m/z 168.19 to identify the presence of SDS. This m/z corresponds to $C_{12}H_{24}$ as reported by (Faust and Abbatt, 2019). It was chosen due to its high signal-to-noise ratio, characterized by a low background concentration and a clear signal

https://doi.org/10.5194/ar-2026-14
Preprint. Discussion started: 5 May 2026
© Author(s) 2026. CC BY 4.0 License.

upon SDS addition, as we had validated by preliminary specific experiments (SI-1). The detailed quantification of SDS and levoglucosan during Exp 4a and 4b can be found in SI-2.

The AMS provided the mass concentration of sulfate ($m_{sulfate}$) and the total mass of organic compounds (m_{org}). The organic to sulfate mass ratio ($f_{o/s} = m_{org}/m_{sulfate}$) was used to track the partitioning of levoglucosan during the experiments. Using this ratio also enabled to correct internally any changes in particle density and collection efficiency during the experiment (provided that the aerosol was internally mixed). Assuming that the organic matter represents levoglucosan with a density of ρ_{org} = 1.69 g cm^{-3}, and taking the ammonium sulfate density (ρ_{AS} = 1.77 g cm^{-3}), the density of the mixed particles $\rho(f_{o/s})$ is a function of $f_{o/s}$ given by Eq. 1:

$$\rho(f_{o/s}) = \frac{\frac{M_{AS}}{M_{sulfate}} + f_{o/s}}{\frac{M_{AS}}{\rho_{AS} M_{sulfate}} + \frac{f_{o/s}}{\rho_{org}}} \quad (1)$$

where M_{AS} is the molar mass of AS; $M_{sulfate}$ is the molar mass of sulfate.

In addition, particles were collected on quartz fiber filters during each experiment. SDS was quantified using the methodology developed in (Grisillon et al., 2026). Briefly, the filter was extracted in 10 mL of ultrapure water, and the resulting solution was filtered using a pre-cleaned polyethylene frit, following the protocol described in (Grisillon et al. 2026). The determination of SDS quantities in the filtrate was performed by colorimetry with ortho toluidine blue, as described in (Grisillon et al. 2026). More details are provided in SI-2.

2.5.2 Size and mass of particles

A Scanning Mobility Particle Sizer (SMPS, TSI, 3081) equipped with X-ray neutralizer (TSI model 3088) and coupled with a Condensation Particle Counter (CPC, TSI, 3772), was connected directly to the CESAM chamber, to measure the size of the wet (deliquesced) particles without pre-drying. The sample flow rate and sheath flow rate were set to 1 L min^{-1} and 10 L min^{-1}, respectively, resulting in a size detection range of 7.64–289 nm for wet particles during the 100 nm dry injected size experiment days. During the 200 nm dry injected size experiment days, a sheath flow of 5 L min^{-1} and an aerosol flow of 1 L min^{-1} were used, yielding a scanned size range of 11.3–461.4 nm.

To monitor the size distribution of dry particles, a TROPOS-style Mobility Particle Size Spectrometer (MPSS) system equipped with a ^{63}Ni neutralizer and coupled with a Nafion dryer was connected to CESAM. The MPSS consisted of two TROPOS-modified Hauke-type Differential Mobility Analyzers (DMA) (Wiedensohler et al., 2012;Winklmayr et al., 1991). A short DMA was used for detecting particles in the small size range (5.1 - 40 nm), with sheath air flow and sample air flow rates set at 15 and 1.5 L min^{-1}, respectively. A long DMA measured particles in the larger size range (20 - 800 nm), with corresponding sheath air flow and sample air flow rates of 5 and 1 L min^{-1}, respectively. An ultrafine condensation particle counter (CPC, TSI 3750) was employed to count aerosols downstream of the short DMA, while a standard condensation particle counter (CPC, TSI 3772) was used for particles from the long DMA. The particle number size distributions across the two size ranges were calculated and merged using the TROPOS inversion routines to produce the final particle number size distribution. All flow rates were continuously monitored and recorded with the same time resolution as the particle size distribution measurements. Further details on the MPSS can be found elsewhere (Birmili et al., 1999;Aalto et al., 2001;Wiedensohler et al., 2012). The SMPS and MPSS were intercalibrated with a CPC (TSI, 3750) in ambient air. The MPSS and the CPC gave

https://doi.org/10.5194/ar-2026-14
Preprint. Discussion started: 5 May 2026
© Author(s) 2026. CC BY 4.0 License.

a good agreement on the number concentration, and this number concentration was 1.2 times higher than that of the SMPS. The MPSS signal was taken as the reference in all experiments.

It was expected that after the Nafion dryer, the RH in the MPSS would be low enough for all particles to dry completely before entering the instrument (which is 40% RH from the ACTRIS recommendations). However, due to technical issues with the dryer, the RH sensor integrated into the sheath flow of the MPSS indicated values ranging from below 15 to 50%, depending on the RH in CESAM and, as a result, the measured particle size was dependent on the internal RH% (as shown in Fig. 2 for Exp 1a). It was thus necessary to adopt a methodology of particle size correction to obtain dry particle size and mass concentrations, even though it provided additional uncertainties, as shown below. The following correction procedure was applied:

1/ based on the study from (Lei et al., 2018) who investigated the water uptake between 15% and 95%RH of AS and levoglucosan mixed particles experimentally and theoretically, we have built a two dimensional matrix of growth factors $g\left(RH_{MPSS}, f_{o/s}\right)$ by interpolating their experimental data, where RH varied from 15% to 95% with a precision of 1% and $f_{o/s}$ varied between 0.45 and 4.12 with a precision of 0.02. More details on the matrix of growth factors $g\left(RH_{MPSS}, f_{o/s}\right)$ can be found in the SI-3.

2/ The growth factor $g\left(RH_{MPSS}, f_{o/s}\right)$ was then used to correct the particle size and total mass concentrations only when RH in the MPSS was higher than 15%. Below 15% RH, no correction was applied.

3/ Assuming that the growth factor did not depend on particle size, the dry particle size and particle mass concentration were calculated according to eq. 2.

$$\begin{cases} D_{ve} = \sqrt[3]{\frac{\sum_{i=1}^{k} n_i \cdot \left(d_i/f_g\right)^3}{\sum_{i=1}^{k} n_i}} = \frac{D_{ve}\_raw}{f_g} \\ m_{total} = \rho\left(f_{o/s}\right)\frac{\pi}{6}\sum_{i=1}^{k} n_i \cdot \left(d_i/f_g\right)^3 \end{cases} \quad (2)$$

$$\text{with} \begin{cases} f_g = 1, if\ RH_{MPSS} < 15\% \\ f_g = g\left(RH_{MPSS}, f_{o/s}\right), if\ 15\% \le RH_{MPSS} \le 95\% \end{cases}$$

where D_{ve} is the volume equivalent diameter under dry conditions in *nm*; D_{ve}_raw is the volume equivalent diameter given by the MPSS in *nm*; k is the bin number of the size distribution given by the MPSS; d_i is the average diameter of each bin in *nm*; n_i is the number concentration of each bin in cm^{-3} ; m_{total} is the total mass concentration of particles under dry conditions in $\mu g\ m^{-3}$; $\rho\left(f_{o/s}\right)$ is the density of particles obtained from Eq. 1; and f_g is the correction factor. The 5% uncertainty on D_{ve}_raw (MPSS default) and the 2% uncertainty on f_g (Lei et al., 2018) result in 7% uncertainty on D_{ve} and 26% on m_{total}. The RH% limits for f_g were chosen based on Fig. S4, which shows that, to limit the bias between the uncorrected and corrected dry mass of particles to below 10%, the RH inside the MPSS must be ≤ 15%.

4/ The mass concentration of ammonium sulfate (m_{AS}) and organic matter (m_{org}) were finally calculated based on m_{total} using the organic to sulfate ratio ($f_{o/s}$) determined by the AMS.

Figure 2 shows the effect of this correction procedure for Exp 1a, performed with pure AS particles. The RH in CESAM decreased from 85% to 38% in two steps (first decrease starting at

https://doi.org/10.5194/ar-2026-14
Preprint. Discussion started: 5 May 2026
© Author(s) 2026. CC BY 4.0 License.

13:45 and the second one at 16:15). The RH in the MPSS clearly followed the same time-profile, decreasing from 35% to 16%. This shows that the efficiency of the Nafion dryer was not sufficient to dry the particles completely. This is confirmed by the comparison between the time profiles of D_{ve}_wet and D_{ve}_dry_raw (Fig. 2, middle panel). Although D_{ve}_wet logically follows the decrease of RH in the chamber, D_{ve}_dry_raw shows a sudden decrease from 100 nm to 90 nm at 14h, corresponding to the efflorescence point of the AS particles. The same behavior happens with the total mass concentrations (Fig. 2, bottom panel).

After applying the procedure, the corrected dry volume-equivalent diameter (D_{ve}_dry_corrected, Fig. 2, middle panel) remains stable at approximately 90 nm throughout the experiment. The corrected dry mass (Mass_dry_corrected, Fig. 2, bottom panel) shows a smooth exponential decrease throughout the experiment, due to the decrease of the particle number concentration. Several data points (pink shaded area in Fig. 2) represent the efflorescence transition when RH in the MPSS ranges from 30 to 33%, in good agreement with the water uptake studies of pure AS particles (Zardini et al., 2008;Vlasenko et al., 2017;Lei et al., 2020;Lei et al., 2018;Zhang et al., 2023). This transition period is removed from the final corrected data. Note that, due to the RH% in the MPSS, four points between 20 and 60 minutes were already in this transition period, they were also removed from the final corrected data.

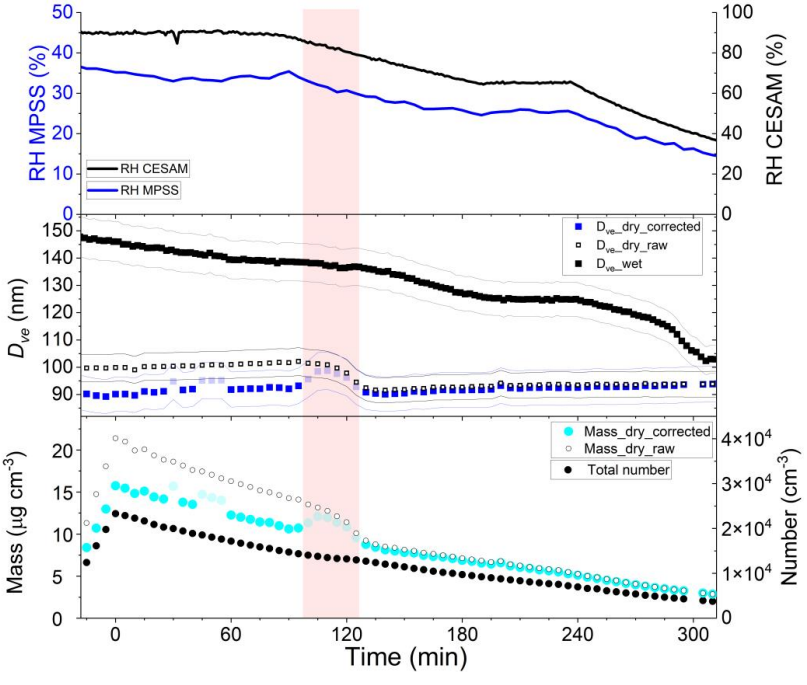

Figure 2 : Comparison between corrected and uncorrected data of dry AS particles under decreasing RH conditions (Exp 1a). Time profiles of RH in CESAM and in the MPSS instrument (top panel), raw (uncorrected) volume equivalent diameter (D_{ve}_dry_raw) and corrected volume equivalent diameter under dry condition (D_{ve}_dry_corrected), and volume equivalent diameter under wet condition (D_{ve}_wet) (middle panel), raw (uncorrected) total mass concentration (Mass_dry_raw), corrected total mass concentration (Mass_dry_corrected), and total number concentration (bottom

https://doi.org/10.5194/ar-2026-14
Preprint. Discussion started: 5 May 2026
© Author(s) 2026. CC BY 4.0 License.

312 panel). The period of efflorescence is shaded pink, and open blue symbols denote the excluded data
313 points

314 These results show the importance of considering the applied correction for the dry size of the
315 particles. Although this correction procedure generated larger uncertainties than direct measurements
316 on the particles mass (26%, Tab. 1), these corrections did not affect $f_{o/s}$ which was used to calculate
317 the net evaporation of levoglucosan from AS particles.

318

319 ### 2.6 Calculation of the net evaporation of levoglucosan from AS particles

320 The net evaporation rate of levoglucosan from the AS particles was determined by measuring
321 the mass concentrations of sulfate and levoglucosan using the AMS. Due to dilution, wall loss
322 processes, and gas-particle partitioning, both concentrations decreased with time, but at different
323 rates:

324 $$[S]_t = [S]_0 \exp(-k_1 t) \quad (3)$$

325 $$[OA]_t = [OA]_0 \exp(-k_2 t) \quad (4)$$

326 where $[S]_t$ is the sulfate mass concentration at time t, and $[OA]_t$ the particle-phase levoglucosan mass
327 concentration at time t (time 0 is the time when the introduction procedure was finished); k_1 is the
328 decay rate constant including wall loss processes and dilution of sulfate, and k_2 the combined decay
329 rate constant of wall loss processes and dilution, as well as gas-particle partitioning of levoglucosan.
330 Combining (1) and (2) gives:

331 $$[OA]_t/[S]_t = [OA]_0/[S]_0 \exp(-k_{net} t) \quad (5)$$

332 where k_{net} is the resulting rate constant: $k_{net} = k_2 - k_1$. Assuming an internal mixture of the particles
333 one can state that the dilution and wall loss processes are the same for both sulfate and particle-phase
334 levoglucosan. As a result, k_{net} is the rate constant representing the net evaporation of levoglucosan
335 from the particles, and its values are positive when levoglucosan evaporates from the particles,
336 whereas they are negative when levoglucosan condenses onto the particles.

337 Absolute uncertainties of k_{net} values (Tab 2) were calculated from their relative uncertainties which
338 was the sum of the relative uncertainties of $f_{o/s}$ and those given by the linear regression of the
339 $Log\ (f_{o/s})$ versus time.

340 ## 3. Results and discussions

341 ### 3.1 Observation of levoglucosan evaporation under various RH%

342 In each experiment, once the particles are introduced, they stabilize and undergo continuous
343 dilution and wall loss, leading to a steady decrease in the mass concentration of each component.
344 Figure 3 shows three experiments performed under different conditions: constant dry 0% RH with
345 ~200 nm injected dry size particles (left panels); decreasing RH starting from > 90% with ~100 nm
346 injected dry size particles (middle panels), and with ~200 nm injected dry size (right panels). The
347 vertical dashed lines correspond to time t = 0. Note that the initial dry size (D_{ve}) at time t = 0 is
348 always below the targeted size (100 or 200 nm) and can vary from one experiment to another due to

https://doi.org/10.5194/ar-2026-14
Preprint. Discussion started: 5 May 2026
© Author(s) 2026. CC BY 4.0 License.

the variable time taken for particle injection (from 1 to 2 hours), during which evaporation already occurred.

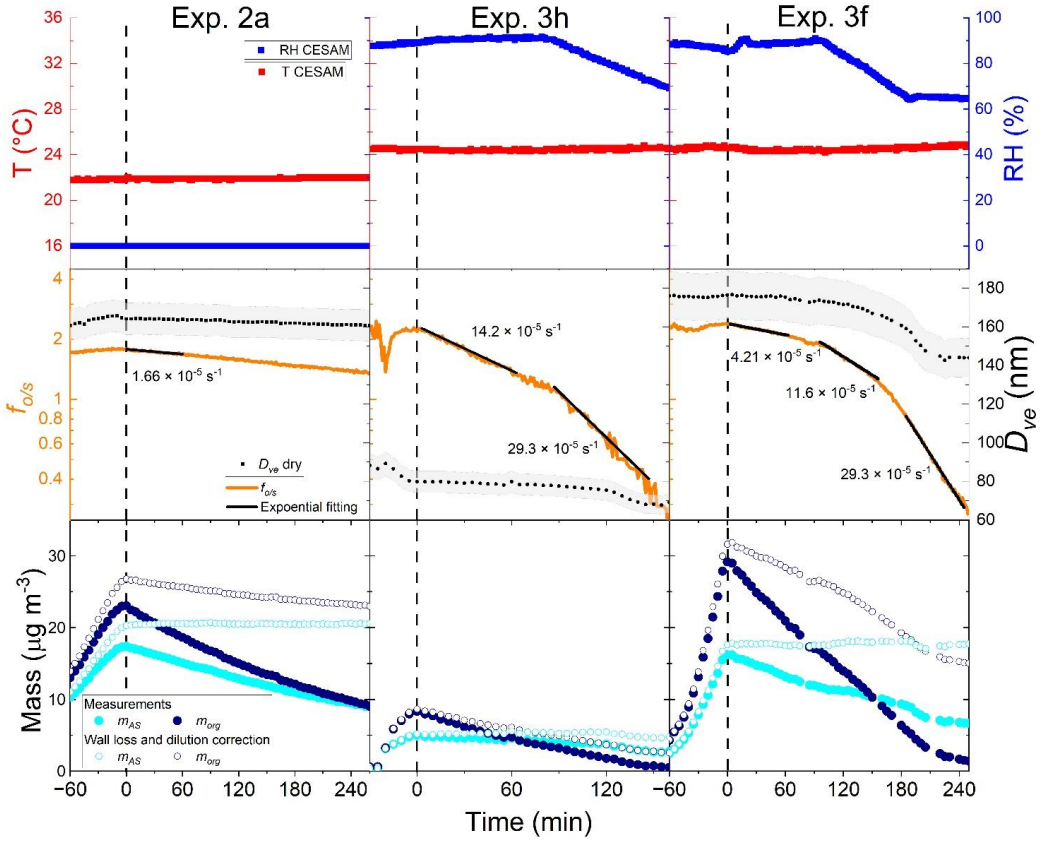

Figure 3. Evaporation of levoglucosan during three experiments performed under different RH and particle monodispersed size conditions: dry 0% RH at ~200 nm (Exp 2a, left column), decreasing RH at ~100 nm (Exp 3h, middle column), and decreasing RH at ~200 nm (Exp 3f, right column). Time series of T, RH (top row), volume equivalent dry particle size (D_{ve}), organic to sulfate mass ratio ($f_{o/s}$) (middle row), masses of AS (m_{AS}) and total organic (m_{org}, attributed to levoglucosan) with and without wall loss and dilution corrections (bottom row). The grey shades show the uncertainty of D_{ve} after correction (see SI-3). The black lines indicate the exponential fitting curves (during 60 min) to determine k_{net} (according to Eq. 5), which values are shown. The vertical dashed line marks time 0, at the end of particle introduction into CESAM.

In all experiments, although T was constant throughout each experiment (Fig. 3, top row), particle shrinking was observed versus time (Fig. 3, middle row, black dots). Initially, when RH was kept constant (dry (Exp 2a) or wet (Exp 3h and 3f just after time 0)), the shrinking was only slight but became significant once RH started to decrease. For example, according to the variation of D_{ve} in Exp 3h (middle panel), a total particle volume of 6.8% was lost in the first 70 min when RH was constant at 89.1 ± 0.6 %, and this value increased to 33% in the next 70 min when RH decreased down

https://doi.org/10.5194/ar-2026-14
Preprint. Discussion started: 5 May 2026
© Author(s) 2026. CC BY 4.0 License.

to 70%. In Exp 3f (right panel), the total volume loss was 5.4% in the first 97 min (RH was constant at 88.9 ± 1.1 %) and increased to 32% in the next 97 min (RH decreased down to 65%).

Figure 3 (bottom rows) shows that, after dilution and wall loss corrections (Doussin et al., 2023), the mass concentrations of AS remained almost constant over time whereas that of levoglucosan (represented by OA) decreased continuously. Thus, the observed particle shrinking versus time was due to the evaporation of levoglucosan. This is consistent with the non-volatility of AS and the significant volatility of levoglucosan. This observation becomes even more obvious in the decrease of the organic to sulfate mass ratio versus time (Fig. 3, middle rows). The organic to sulfate mass ratio constantly decreases versus time under constant RH, and it decreases at a significantly higher rate when RH decreases. This is reflected by the net evaporation rate (k_{net}) values, calculated from the decrease of the organic to sulfate mass ratio. For each experiment, k_{net} shows higher values when RH decreases than when it is constant. For instance, at ~100 nm dry size (Exp 3h, middle column), k_{net} increases by a factor of 2.1 (from 14×10^{-5} s^{-1} to 29×10^{-5} s^{-1}) when RH decreases from 92% to 70%; at ~200 nm dry size (Exp 3f, right column), k_{net} increases by a factor of 2.8 (from 4.2×10^{-5} s^{-1} to 12×10^{-5} s^{-1}) when RH decreases from 90% to 65%. The factors influencing this net evaporation rate will be discussed in detail in section 3.3.

3.2 Co-condensation of levoglucosan

Due to the high deliquescence RH of AS, all the experiments conducted under humid conditions were initialized at RH above 80%, then, RH either remained constant or decreased over time (Table 1). However, in one experiment (3d), we were successful in increasing the relative humidity to 100% after the particle injection. Note that, although the very high relative humidity, no cloud formation was observed in CESAM, as shown by the absence of particle washout (Giorio et al., 2017). This appeared to impact the trend in the organic-to-sulfate mass ratio. As shown in Fig. 4, an increase in RH from 88% to 100% coincided with a rise in the organic to sulfate mass ratio from 2.1 to 2.2, suggesting that levoglucosan was co-condensing with water vapor. This effect is further supported by dry MPSS measurements, which show a slight increase in the corrected dry D_{ve} during RH increase. Note however that this increase continues even when the RH stabilizes. This disagrees with the change in $f_{o/s}$ evolution after 60 minutes in Fig. 4. It is probably due to the uncertainties generated by the dry D_{ve} corrections, which however do not affect $f_{o/s}$ values (see section 2.5.2).

Using Eq. 5 to calculate k_{net} (see Sect. 2.6), a negative value of -1.15 ($\pm$ 0.11) $\times10^{-5}$ s^{-1} was determined by fitting the organic to sulfate mass ratios ($f_{o/s}$ in Fig. 4, middle row) during the RH increase. This indicates condensation of levoglucosan, as evidenced by the negative sign of the rate constant and the fact that its magnitude significantly exceeds the uncertainty. Furthermore, the absolute value of this co-condensation rate constant is in the range of the fitted net evaporation rate constants obtained in other experiments which span from 0.91×10^{-5} up to 29 $\times10^{-5}$ s^{-1} (Table 1). However, given the likely significant competitive uptake of gas-phase levoglucosan onto the chamber walls (Lamkaddam et al., 2017), the calculated co-condensation rate constant is likely influenced by the substantial wall losses, the full quantification of which is out of the scope of the present study.

https://doi.org/10.5194/ar-2026-14
Preprint. Discussion started: 5 May 2026
© Author(s) 2026. CC BY 4.0 License.

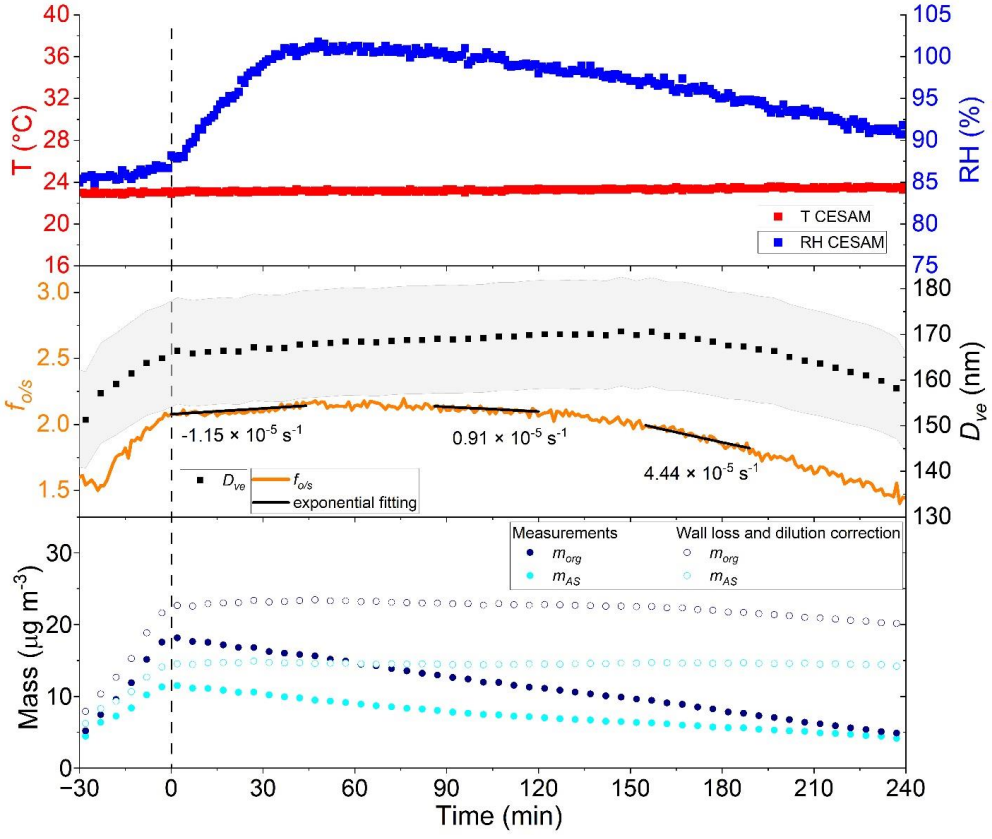

Figure 4. Co-condensation, then evaporation of levoglucosan during experiment 3d, performed under varying RH. Time series of T, RH% (top panel), volume equivalent dry particle size (D_{ve}), organic to sulfate mass ratio ($f_{o/s}$) (middle panel), ammonium sulfate and total organic (attributed to levoglucosan) masses (with and without wall loss and dilution corrections) (bottom panel). The grey shades show the uncertainty of D_{ve} after correction (see SI-3). The three black lines indicate the exponential fitted curve to determine k_{net} values (shown) during 45 min when RH increases, and 40 min when RH stays constant, and decreases, respectively. The vertical dashed line marks time 0, at the end of particle introduction in CESAM.

3.3 Factors driving the net evaporation rate constant of levoglucosan

Figs. 3 and 4 clearly demonstrate the evaporation and condensation of levoglucosan from and onto AS particles for several experiments. Yet, it seems that the extent of these phenomena is linked to multiple factors, not only the variations in RH. In this section, we discuss the influence of the measured parameters on the partitioning of levoglucosan. Figure 5 shows the values of k_{net} versus each of the investigated parameters across all experiments.

https://doi.org/10.5194/ar-2026-14
Preprint. Discussion started: 5 May 2026
© Author(s) 2026. CC BY 4.0 License.

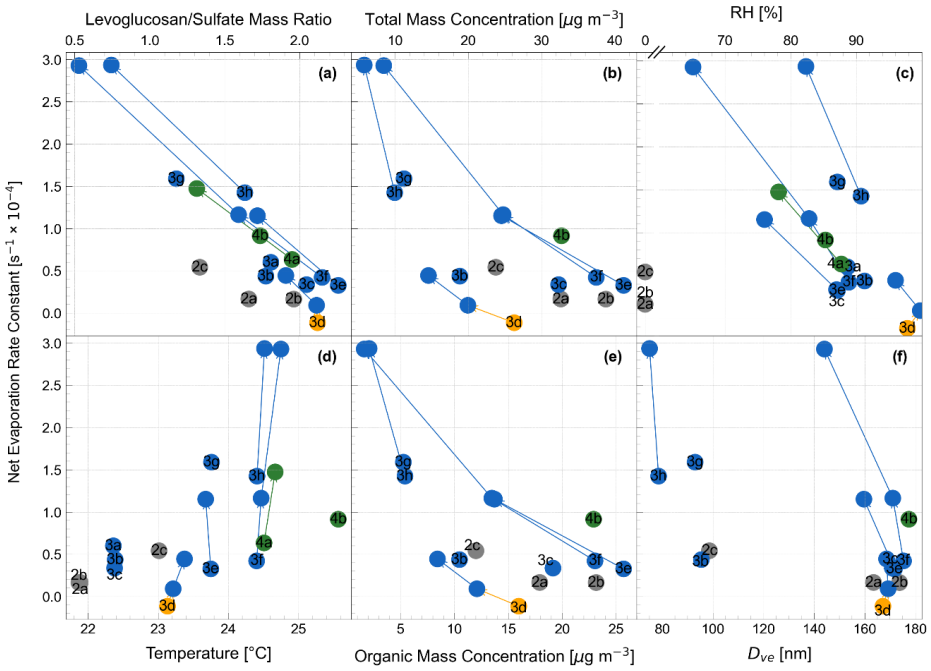

Figure 5. Net levoglucosan evaporation rate constant k_{net} as a function of levoglucosan to sulfate mass ratio (a), total mass concentration (b), RH (c), temperature (d), organic mass concentration (e) and particle dry diameter (f). Exp 2a, 2b, 2c (gray dots) were performed under dry conditions (RH = 0%). Exp 4a and 4b (green dots) involve SDS. Blue dots represent experiments performed at high initial RH either constant or decreasing. The orange dots correspond to the 1st part of Exp 3d, when RH increased from 88 to 100% (Sect. 3.2). The arrows connect experiments performed under varying RH conditions, their arrowheads pointing towards increasing time. k_{net} are plotted at the middle value for parameters that change during the evaluation period (i.e. all parameters except from T).

Overall, Fig. 5 shows that k_{net} values are largely influenced by the mass ratio of levoglucosan to sulfate (Fig. 5a). A general trend is observed where lower levoglucosan-to-sulfate ratios correspond to higher k_{net} values, potentially due to a salting-out effect. As the experiment progresses and levoglucosan volatilizes, the proportion of AS in the particles increases, which likely enhances the salting-out effect, thereby accelerating the volatilization rate. AS has been reported to exhibit a salting-out effect for polyol/water mixtures (Marcolli and Krieger, 2006). This effect, which depends on the oxygen-to-carbon ratio (Song et al., 2012), the molecular structure of the organic molecules, and the organic-to-sulfate mass ratio (Bertram et al., 2011) likely enhances the evaporation (Angle et al., 2023).

In addition to the levoglucosan-to-sulfate mass ratio, RH (Fig. 5c), particle size (Fig. 5f) and temperature (Fig. 5d) also influence the k_{net} values. Under dry conditions (Exp 2a and 2b), the k_{net} values are among the lowest positive values compared to particles of similar size under higher RH (Fig. 5f). This can be explained by the fact that levoglucosan effloresces at very dry conditions in the presence of crystalline AS (Parsons et al., 2004), and, as a crystalline solid it has a lower vapor pressure compared with the supersaturated solutions (Booth et al., 2011). Moreover, it is possible that levoglucosan forms an external mixture with AS in Exp 2a, 2b and 2c, this would explain why

https://doi.org/10.5194/ar-2026-14
Preprint. Discussion started: 5 May 2026
© Author(s) 2026. CC BY 4.0 License.

450 k_{net} of these experiments do not align well with the others in Fig. 5a. However, Exp 2a and 2b were
451 performed under the lowest temperature, which also influences k_{net} values: Fig. 5d shows that
452 increasing T provides higher k_{net} values. For wet particles, Fig. 5c shows that decreasing RH
453 systematically results in higher k_{net} values, thus potentially indicating co-evaporation of levoglucosan.
454 Also, larger particles are associated with slower volatilization rates (Fig. 5f) due to their decreasing
455 surface/volume ratios with increasing size. In the same way, lower total mass (Fig. 5b) is associated
456 with higher evaporation, consistently with evaporation being exacerbated by N_2 dilution in the
457 chamber.

458 Overall, the lowest positive k_{net} values (with a corresponding half-life of approximately 12
459 hours) are observed when the levoglucosan-to-sulfate mass ratio is highest, and either RH is high (>
460 80 %) or the temperature is low. The highest k_{net} values (with a corresponding half-life of
461 approximately 1 hour) occur when the levoglucosan-to-sulfate mass ratio is lowest, and either RH is
462 low or temperature is high.

463 The analysis above demonstrates physical trends, but it is difficult to isolate the individual
464 effects of each parameter, as they are not completely independent. To elucidate their combined
465 influence on the k_{net} values and investigate their interrelationships, we constructed a Pearson pairwise
466 linear correlation matrix derived from the original datasets shown in Fig. 5 for Exp 3b to 3h (see SI-
467 4 for the details). Exp 3a was excluded from this matrix due to the lack of data for D_{ve}, m_{org} and m_{total}.
468 Furthermore, Exp 4a and 4b were done under different conditions (with the presence of SDS) and
469 are treated separately in the next section. The resulting matrix is shown in Figure 6.

470

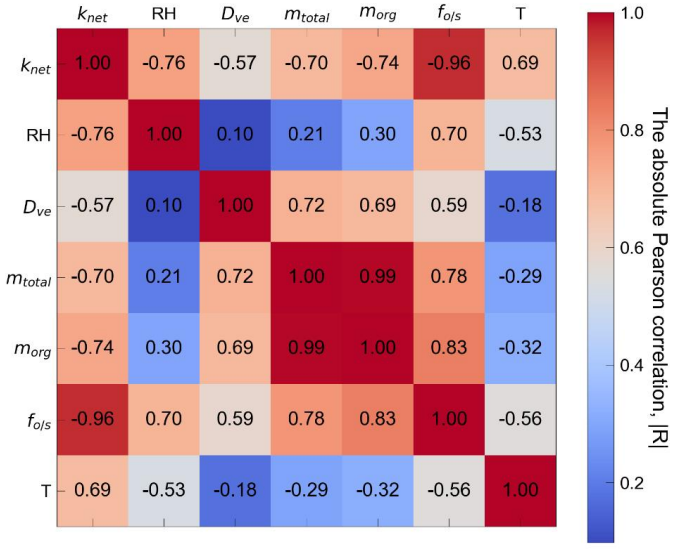

471

472 **Figure 6.** Correlation matrix showing pairwise Pearson correlation coefficients among the
473 investigated parameters and the net evaporation rate k_{net} for Exp 3b to 3h. D_{ve} is the dry volume
474 equivalent particle size; m_{total} is the total mass concentration; m_{org} is the organic mass concentration,
475 $f_{o/s}$ is organic-to-sulfate mass ratio; T is the temperature.

https://doi.org/10.5194/ar-2026-14
Preprint. Discussion started: 5 May 2026
© Author(s) 2026. CC BY 4.0 License.

AEROSOL Research Discussions

The resulting matrix (Figure 6) clearly reveals that, under our experimental conditions, the levoglucosan-to-sulfate mass ratio serves as the dominant factor governing the volatilization rate of levoglucosan. RH emerges as the second most influential parameter, closely followed by the organic mass and the total mass, demonstrating their importance. The dry particle size and temperature appear to be the least influential parameters on k_{net} values, but their absolute Pearson correlations are still higher than 0.5.

As mentioned above, the strong influence of the levoglucosan-to-sulfate mass ratio can be explained by the salting-out effect that is strengthened when the proportion of salt increases while levoglucosan evaporates from the particles. Remarkably, RH is independent of all parameters except the two linked parameters, $f_{o/s}$ and k_{net}. This demonstrates that levoglucosan co-evaporates (or co-condenses) with water in these experiments. In Fig 6, Exp 4a and 4b were excluded as they were performed under different conditions (SDS presence), they are discussed below.

3.4 Influence of the presence of SDS

Two experiments, Exp 4a and 4b, were performed with addition of SDS, to investigate the impact of a surfactant on levoglucosan partitioning. As a surfactant, SDS is expected to form a layer on the surface of the particle, potentially affecting the partitioning of both water and levoglucosan. However, as seen in Fig. 5, the presence of SDS does not seem to impact the k_{net} values. This suggests that the presence of SDS does not affect the net evaporation of levoglucosan. Contrasting results have been reported in previous studies on the effect of SDS on the kinetics of water evaporation. Experiments performed by (Taflin et al. 1988) and (Shulman et al. 1997) indicated that the presence of SDS slows down the evaporation of water. However, other studies suggested that SDS has no effect on the kinetics of water evaporation (Davies et al. 2012; Doganci et al. 2011; Lunkenheimer et Zembala 1997). Davies et al. (2012) explain their results with the large, charged head group of SDS, which is unlikely to provide a densely packed monolayer of SDS at the surface. More generally, soluble surfactants such as SDS seem to have little effects on the evaporation of water (Lunkenheimer et Zembala 1997). According to (Doganci et al. 2011), two competing effects arise from the presence of SDS: i) surface tension reduction would promote water evaporation, and ii) the presence of SDS molecules at the surface would hinder molecules diffusion and thus impede water evaporation. However, to account for these effects, the surface tension and surface coverage of SDS must be estimated in Exp 4a and 4b.

In the particle, surfactant SDS molecules partition between the 'interior' of the particle – the bulk – and the surface. The bulk concentration of SDS and its surface coverage were estimated from the total SDS concentration in the particle and the geometry of the particle, following the methodology proposed by (Jacobs et al. 2024). This methodology accounts for the high surface area – to – volume ratios of small particles (see Table 2). The SDS concentration is calculated from both AMS data and the filters collected during the experiments, and using the wet particle D_{ve} obtained from the SMPS. More details on the calculations can be found in SI-2. The results are shown in Table 2 at three and two time-steps for Exp 4a and 4b, respectively.

The results presented in Table 2 for filters and AMS are approximate estimations, due to the uncertainty on AMS derived SDS concentration (see SI-2-1) and because the exact flow rate of filter sampling was not precisely controlled (see SI-2-2). For Exp 4b, there is close agreement between the values obtained from AMS data and filter data. However, there is a significant difference between

https://doi.org/10.5194/ar-2026-14
Preprint. Discussion started: 5 May 2026
© Author(s) 2026. CC BY 4.0 License.

519 the results from the AMS and the filter for Exp 4a, with a factor 5-7 for the estimated total
520 concentration in the particle. This leads to significant differences between the bulk concentrations,
521 surface coverages, and surface tension calculated from AMS and filter data, although these
522 differences can arise from the uncontrolled sampling flow rate or the uncertainty on AMS derived
523 SDS concentration (see SI-2-1). In particular, the bulk concentration is predicted to be below the
524 CMC during experiment 4a according to filter data, whereas AMS predicts a bulk concentration
525 above the CMC. This explains the discrepancies between AMS and filter data for surface coverage
526 and surface tension. Note that the surface tension data used for these estimations do not account for
527 the presence of ammonium sulfate in the particle, which can greatly impact bulk – surface
528 partitioning due to salting-out effects (El Haber et al., 2023). Therefore, the surface coverages and
529 surface tensions estimated in Table 2 can be considered as lower limits and upper limits of the true
530 values, respectively.

531

532 **Table 2.** SDS experiments (Exp 4a and 4b): estimated surface-to-volume (A/V) ratios, SDS
533 concentrations in the particle, surface coverages by SDS (detailed in SI-2). SDS concentration and
534 surface coverages were calculated from both AMS and filter data. A/V ratios and results calculated
535 from AMS data were averaged for the first 10 min of experiments after each indicated time.

Exp no.		**4a**			**4b**	
Time (min)		19	93	153	0	49
k_{net} (min^{-1})		$3.8.10^{-3}$	$3.8.10^{-3}$	$8.8.10^{-3}$	$5.5.10^{-3}$	$5.5.10^{-3}$
A/V ratio (x 10^6 m^{-1})		23.1	23.3	26.9	26.9	26.9
Wet D_{ve} (nm)		260	257	223	248	261
SDS total concentration (x 10 mmol L^{-1})	**AMS**	39	55	88	93	61
	Filter	8.5	8.8	13	114	69
SDS bulk concentration (x 10 mmol L^{-1})	**AMS**	14	29	58	62	36
	Filter	0.16	0.16	0.25	84	44
Levoglucosan concentration (mol/L)		1.1	1.1	1.2	2	1.3
AS concentration (mol/L)		1.4	1.8	3.1	2.5	2.1
SDS surface coverage (%)	**AMS**	98	99	99	100	99
	Filter	32	33	43	99	99
Surface tension (mN m^{-1})	**AMS**	35	35	35	35	35
	Filter	61	61	56	35	35

536

537 Overall, the estimations suggest that particles were indeed coated with SDS, and that surface tension
538 was reduced compared to pure water. Nevertheless, the net evaporation of levoglucosan seems to be
539 unaffected by this coating and surface tension reduction, as shown in Fig. 5. This suggests that these
540 two effects counteract, as suggested by (Doganci et al. 2011), or that even at high surface coverages,
541 SDS is not tightly packed enough to prevent water molecules diffusion. In addition, note that the
542 bulk SDS concentrations are smaller than the levoglucosan and AS concentrations, suggesting that
543 bulk SDS has a small impact on bulk properties and thus on k_{net}. Moreover, although our calculations
544 predict full coverage of SDS, it is possible that surfactants are not evenly distributed across the
545 surface, i.e. that surface concentration is not homogeneous. (Griffith et al. 2012) showed that

https://doi.org/10.5194/ar-2026-14
Preprint. Discussion started: 5 May 2026
© Author(s) 2026. CC BY 4.0 License.

surfactants can exhibit heterogeneity at the surface, with regions of 3D hydrophobic aggregates, condensed monolayer, or exposed hydrophilic "holes", where the solute is at the surface in place of surfactant molecules. Although the surfactant used in the latter study was not SDS, it is still possible that the particle surface presents such hydrophilic holes due to the presence of levoglucosan, leading to unaffected levoglucosan evaporation.

4. Conclusions and atmospheric implications

The ability of a semi-volatile water-soluble organic compound to co-condense and co-evaporate onto or from inorganic particles was investigated. The gas-particle partitioning of levoglucosan was monitored under ambient-like conditions on ammonium sulfate (AS) monodispersed particles in the CESAM simulation chamber. Various conditions were explored, including RH (from dry to 100%), particle mass and size, and the presence of a surfactant on the particles. The net evaporation flux of levoglucosan was quantified under each condition.

Due to the high deliquescence point of AS, wet experiments were initialized at RH above 80%. In these experiments, special care was taken with RH control and measurements. To maintain high RH values in the chamber while preventing liquid water from depositing on the walls, the HUMidificAtioN System (HUMANS) was connected to CESAM to regulate RH precisely. The saturation water vapor pressure and the water vapor pressure were derived from the Buck equation, using the dew point (measured by a chilled mirror) and the average temperature (provided by three thermocouples Type T sensors suspended in the air inside CESAM), respectively. RH was calculated as the ratio between these two vapor pressures. All these precautions made it possible to perform experiments under constant high RH for minutes to hours (and as high as 100%), with a precise control of RH variations. It was shown that these long-time high RH conditions impacted the drying process required to determine the dry volume equivalent diameter of the particles. To achieve this under our experimental conditions, the RH limit value was set at 15% for all experiments.

The results showed that the net evaporation rate of levoglucosan was sensitive to all the investigated parameters, but the main drivers under our experimental conditions were the levoglucosan-to-sulfate mass ratios and RH. The effect of the levoglucosan-to-sulfate mass ratios was interpreted as the increasing salting-out effect of the organic fraction while decreasing the particle water content. The influence of RH provides experimental proof of co-evaporation or co-condensation of levoglucosan from or onto AS particles.

To investigate the impact of a surfactant on levoglucosan partitioning, out of the fifteen experiments, two were performed with addition of sodium dodecyl sulfate (SDS) under wet conditions. As a surfactant, SDS was expected to form a layer on the surface of the particle, potentially affecting the partitioning of both water and levoglucosan. The quantification of SDS in the particles made it possible to estimate that particles were indeed coated with SDS, and that surface tension was reduced compared to pure water. Nevertheless, compared to the thirteen other experiments, the net evaporation of levoglucosan seemed to be unaffected by this coating and surface tension reduction. This result was interpreted as the counteracting effects of coating and surface tension reduction, and/or as the potential heterogeneity of SDS molecules at the particle surface, inducing, in some places, a lack of packing tightness of the SDS layer to inhibit diffusion across it. These showed that more investigations should be carried out on the effect of surfactants on the

https://doi.org/10.5194/ar-2026-14
Preprint. Discussion started: 5 May 2026
© Author(s) 2026. CC BY 4.0 License.

partitioning of semi-volatile organic compounds, using various types of surfactants and investigating observations of the surface properties.

Overall, the results showed that the net evaporation flux of levoglucosan for particle-phase levoglucosan corresponds to atmospheric lifetimes of 1 to 12 hours, which is comparable to the photochemical degradation rates of the particle phase (approximately 17 hours) at similar temperatures. This result highlights the importance of considering the phase partitioning of semi-volatile compounds when assessing their atmospheric multiphase reactivity.

These findings should be followed up with consideration of the co-evaporation or co-condensation of organic, semi-volatile, water-soluble species when determining the CCN ability of particles. A modeling study of these data is also required.

Author Contributions

JX, JW and AM wrote the article. JX, BTR, Julien K, JG, MGS, SD, SH, EP, and KZA participated in the CESAM chamber campaign that was coordinated by JW, BPV, MC, and AM. JX processed and interpreted the data with support from JW, BTR, Judith K, NB and supervised by AM. JG and FRP analyzed and interpreted the surfactants data. KZA, CM, and AM secured funding for the ORACLE project. All co-authors reviewed the article.

Data availability

The data that support the findings of this study are openly available in ACTRIS DC ASC Unit (also called EUROCHAMP DC) https://www.eurochamp.org/).

Notes

The authors declare no conflict of interest.

Acknowledgement

The authors acknowledge funding support from the French National Research Agency (ANR-PRCI; ANR-20-CE93-0008-01 ACT) and the Swiss National Science Foundation (SNSF #197149) for the bilateral research project ORACLE. This work is part of a Transnational access project that is supported by the European Commission under the Horizon 2020 – Research and Innovation Framework Programme, H2020-INFRAIA-2020-1, ATMO-ACCESS Grant Agreement number: 101008004. The authors gratefully acknowledge CNRS-INSU for supporting CESAM platform as a component of the ACTRIS Research Infrastructure. They also thank AERIS (https://www.aeris-data.fr/) for curing and distributing the data within EUROCHAMP Data Center. The authors also acknowledge funding support from the CNRS-INSU program LEFE-CHAT (SURFACT project), and the IRC CNRS – U. Arizona grant (INSPIRE project)

https://doi.org/10.5194/ar-2026-14
Preprint. Discussion started: 5 May 2026
© Author(s) 2026. CC BY 4.0 License.

References

Aalto, P., Hämeri, K., Becker, E., Weber, R., Salm, J., Mäkelä, J. M., Hoell, C., O'dowd, C. D., Hansson, H.-C., Väkevä, M., Koponen, I. K., Buzorius, G., and Kulmala, M.: Physical characterization of aerosol particles during nucleation events, Tellus B: Chemical and Physical Meteorology, 53, 344-358, 10.3402/tellusb.v53i4.17127, 2001.

Alfarra, M. R., Prevot, A. S. H., Szidat, S., Sandradewi, J., Weimer, S., Lanz, V. A., Schreiber, D., Mohr, M., and Baltensperger, U.: Identification of the Mass Spectral Signature of Organic Aerosols from Wood Burning Emissions, Environmental Science & Technology, 41, 5770-5777, 10.1021/es062289b, 2007.

Angle, K. J., Nowak, C. M., and Grassian, V. H.: Organic acid evaporation kinetics from aqueous aerosols: implications for aerosol buffering capacity in the atmosphere, Environmental Science: Atmospheres, 3, 316-327, 10.1039/D2EA00092J, 2023.

Bertram, A. K., Martin, S. T., Hanna, S. J., Smith, M. L., Bodsworth, A., Chen, Q., Kuwata, M., Liu, A., You, Y., and Zorn, S. R.: Predicting the relative humidities of liquid-liquid phase separation, efflorescence, and deliquescence of mixed particles of ammonium sulfate, organic material, and water using the organic-to-sulfate mass ratio of the particle and the oxygen-to-carbon elemental ratio of the organic component, Atmos. Chem. Phys., 11, 10995-11006, 10.5194/acp-11-10995-2011, 2011.

Bhattarai, H., Saikawa, E., Wan, X., Zhu, H., Ram, K., Gao, S., Kang, S., Zhang, Q., Zhang, Y., Wu, G., Wang, X., Kawamura, K., Fu, P., and Cong, Z.: Levoglucosan as a tracer of biomass burning: Recent progress and perspectives, Atmospheric Research, 220, 20-33, 10.1016/j.atmosres.2019.01.004, 2019.

Birmili, W., Stratmann, F., and Wiedensohler, A.: Design of a dma-based size spectrometer for a large particle size range and stable operation, Journal of Aerosol Science, 30, 549-553, 10.1016/S0021-8502(98)00047-0, 1999.

Booth, A. M., Montague, W. J., Barley, M. H., Topping, D. O., McFiggans, G., Garforth, A., and Percival, C. J.: Solid state and sub-cooled liquid vapour pressures of cyclic aliphatic dicarboxylic acids, Atmos. Chem. Phys., 11, 655-665, 10.5194/acp-11-655-2011, 2011.

Buck, A. L.: New Equations for Computing Vapor Pressure and Enhancement Factor, J. App. Meteo. Clim. 20, 1527-1532, 10.1175/1520-0450(1981)020<1527:NEFCVP>2.0.CO;2, 1981.

Davies, J. F., Haddrell, A. E., Miles, R. E. H., Bull, C. R., Reid, J. P.: . Bulk, Surface, and Gas-Phase Limited Water Transport in Aerosol, the Journal of Physical Chemistry A 116 (45): 10987-98, 10.1021/jp3086667, 2012.

DeCarlo, P. F., Slowik, J. G., Worsnop, D. R., Davidovits, P., and Jimenez, J. L.: Particle Morphology and Density Characterization by Combined Mobility and Aerodynamic Diameter Measurements. Part 1: Theory, Aerosol Science and Technology, 38, 1185-1205, 10.1080/027868290903907, 2004.

DeCarlo, P. F., Kimmel, J. R., Trimborn, A., Northway, M. J., Jayne, J. T., Aiken, A. C., Gonin, M., Fuhrer, K., Horvath, T., Docherty, K. S., Worsnop, D. R., and Jimenez, J. L.: Field-Deployable, High-Resolution, Time-of-Flight Aerosol Mass Spectrometer, Analytical Chemistry, 78, 8281-8289, 10.1021/ac061249n, 2006.

Doganci, M. D., Sesli, B. U., Erbil, H. Y. Diffusion-controlled evaporation of sodium dodecyl sulfate solution drops placed on a hydrophobic substrate, Journal of Colloid and Interface Science 362 (2): 524-31, 10.1016/j.jcis.2011.06.060, 2011.

Donahue, N. M., Robinson, A. L., Stanier, C. O., and Pandis, S. N.: Coupled Partitioning, Dilution, and Chemical Aging of Semivolatile Organics, Environmental Science & Technology, 40, 2635-2643, 10.1021/es052297c, 2006.

Doussin, J.-F., Fuchs, H., Kiendler-Scharr, A., Seakins, P., and Wenger, J.: A practical guide to atmospheric simulation chambers, Springer Nature, 2023.

Drewnick, F., Hings, S. S., DeCarlo, P., Jayne, J. T., Gonin, M., Fuhrer, K., Weimer, S., Jimenez, J. L., Demerjian, K. L., Borrmann, S., and Worsnop, D. R.: A New Time-of-Flight Aerosol Mass Spectrometer (TOF-AMS)—Instrument Description and First Field Deployment, Aerosol Science and Technology, 39, 637-658, 10.1080/02786820500182040, 2005.

El Haber, M., Ferronato, C., Giroir-Fendler, A., Fine, L., Nozière, B. : Salting out, non-ideality and synergism enhance surfactant efficiency in atmospheric aerosols, Scientific Reports, 13(1), 20672 - 20672 10.1038/s41598-023-48040-5, 2023.

https://doi.org/10.5194/ar-2026-14
Preprint. Discussion started: 5 May 2026
© Author(s) 2026. CC BY 4.0 License.

Faust, J. A., and Abbatt, J. P. D.: Organic Surfactants Protect Dissolved Aerosol Components against Heterogeneous Oxidation, The Journal of Physical Chemistry A, 123, 2114-2124, 10.1021/acs.jpca.9b00167, 2019.

Giorio, C., Monod, A., Brégonzio-Rozier, L., DeWitt, H. L., Cazaunau, M., Temime-Roussel, B., Gratien, A., Michoud, V., Pangui, E., Ravier, S., Zielinski, A. T., Tapparo, A., Vermeylen, R., Claeys, M., Voisin, D., Kalberer, M., and Doussin, J. F.: Cloud Processing of Secondary Organic Aerosol from Isoprene and Methacrolein Photooxidation, *The Journal of Physical Chemistry A, 121* (40), 7641-7654, 10.1021/acs.jpca.7b05933, 2017

Griffith, E. C., Adams, E. M., Allen, H. C., Vaida V.: Hydrophobic Collapse of a Stearic Acid Film by Adsorbed l-Phenylalanine at the Air–Water Interface, the Journal of Physical Chemistry B 116 (27): 7849-57, 10.1021/jp303913e, 2012.

Grisillon, J., Michel, L., de Barry, J., Nozière, B., Dron, J., Monod, A., and Robert-Peillard, F.: Quantification of four classes of amphiphilic surfactants by solid phase extraction and spectrophotometric detection at nanomolar levels: environmental applications, Talanta, 297, 128575, 10.1016/j.talanta.2025.128575, 2026.

Heikkinen, L., Partridge, D. G., Blichner, S., Huang, W., Ranjan, R., Bowen, P., Tovazzi, E., Petäjä, T., Mohr, C., and Riipinen, I.: Cloud response to co-condensation of water and organic vapors over the boreal forest, Atmos. Chem. Phys., 24, 5117-5147, 10.5194/acp-24-5117-2024, 2024.

Hennigan, C. J., Sullivan, A. P., Collett Jr, J. L., and Robinson, A. L.: Levoglucosan stability in biomass burning particles exposed to hydroxyl radicals, Geophysical Research Letters, 37, 10.1029/2010GL043088, 2010.

Ijaz, A., Temime-Roussel, B., Kammer, J., Mao, J., Simpson, W., Law, K. S., and D'Anna, B.: In situ measurements of gas–particle partitioning of organic compounds in Fairbanks, Faraday Discussions, 258, 23-39, 10.1039/D4FD00175C, 2025.

Jacobs, M. I., Johnston, M. N., and Mahmud, S.: Exploring How the Surface-Area-to-Volume Ratio Influences the Partitioning of Surfactants to the Air–Water Interface in Levitated Microdroplets, The Journal of Physical Chemistry A, 128, 9986-9997, 10.1021/acs.jpca.4c06210, 2024.

Kulmala, M., Laaksonen, A., Korhonen, P., Vesala, T., Ahonen, T., and Barrett, J. C.: The effect of atmospheric nitric acid vapor on cloud condensation nucleus activation, Journal of Geophysical Research: Atmospheres, 98, 22949-22958, 10.1029/93JD02070, 1993.

Kulmala, M., Laaksonen, A., J.Charlson, R., and Korhonen, P.: Clouds without supersaturation, Nature, 388, 336-337, 10.1038/41000, 1997.

Lamkaddam, H., Gratien, A., Pangui, E., Cazaunau, M., Picquet-Varrault, B., and Doussin, J.-F.: High-NOx Photooxidation of n-Dodecane: Temperature Dependence of SOA Formation, Environmental Science & Technology, 51, 192-201, 10.1021/acs.est.6b03821, 2017.

Lee, T., Sullivan, A. P., Mack, L., Jimenez, J. L., Kreidenweis, S. M., Onasch, T. B., Worsnop, D. R., Malm, W., Wold, C. E., Hao, W. M., and Collett, J. L.: Chemical Smoke Marker Emissions During Flaming and Smoldering Phases of Laboratory Open Burning of Wildland Fuels, Aerosol Science and Technology, 44, i-v, 10.1080/02786826.2010.499884, 2010.

Lei, T., Zuend, A., Cheng, Y., Su, H., Wang, W., and Ge, M.: Hygroscopicity of organic surrogate compounds from biomass burning and their effect on the efflorescence of ammonium sulfate in mixed aerosol particles, Atmos. Chem. Phys., 18, 1045-1064, 10.5194/acp-18-1045-2018, 2018.

Lei, T., Ma, N., Hong, J., Tuch, T., Wang, X., Wang, Z., Pöhlker, M., Ge, M., Wang, W., Mikhailov, E., Hoffmann, T., Pöschl, U., Su, H., Wiedensohler, A., and Cheng, Y.: Nano-hygroscopicity tandem differential mobility analyzer (nano-HTDMA) for investigating hygroscopic properties of sub-10 nm aerosol nanoparticles, Atmos. Meas. Tech., 13, 5551-5567, 10.5194/amt-13-5551-2020, 2020.

Lopez, B., Bhattacharyya, N., DeVivo, J., Wang, M., Caudillo-Plath, L., Surdu, M., Bianchi, F., Brasseur, Z., Buchholz, A., Chen, D., Duplissy, J., He, X.-C., Hofbauer, V., Mahfouz, N., Makhmutov, V., Marten, R., Mentler, B., Philippov, M., Schervish, M., Wang, D. S., Weber, S. K., Welti, A., El Haddad, I., Lehtipalo, K., Kulmala, M., Worsnop, D., Kirkby, J., Mauldin, R. L., Stolzenburg, D., Schobesberger, S., Flagan, R., and Donahue, N. M.: A diagonal volatility basis set to assess the condensation of organic vapors onto particles, Environmental Science: Atmospheres, 5, 1035-1061, 10.1039/D5EA00062A, 2025.

https://doi.org/10.5194/ar-2026-14
Preprint. Discussion started: 5 May 2026
© Author(s) 2026. CC BY 4.0 License.

Lunkenheimer, K., Zembala, M., Attempts to Study a Water Evaporation Retardation by Soluble Surfactants , Journal of Colloid and Interface Science 188 (2): 363-71, 10.1006/jcis.1997.4781, 1997.
Marcolli, C., and Krieger, U. K.: Phase Changes during Hygroscopic Cycles of Mixed Organic/Inorganic Model Systems of Tropospheric Aerosols, The Journal of Physical Chemistry A, 110, 1881-1893, 10.1021/jp0556759, 2006.
Parsons, M. T., Knopf, D. A., and Bertram, A. K.: Deliquescence and Crystallization of Ammonium Sulfate Particles Internally Mixed with Water-Soluble Organic Compounds, The Journal of Physical Chemistry A, 108, 11600-11608, 10.1021/jp0462862, 2004.
Pye, H. O. T., Zuend, A., Fry, J. L., Isaacman-VanWertz, G., Capps, S. L., Appel, K. W., Foroutan, H., Xu, L., Ng, N. L., and Goldstein, A. H.: Coupling of organic and inorganic aerosol systems and the effect on gas–particle partitioning in the southeastern US, Atmos. Chem. Phys., 18, 357-370, 10.5194/acp-18-357-2018, 2018.
Qin, C., Gou, Y., Wang, Y., Mao, Y., Liao, H., Wang, Q., and Xie, M.: Gas–particle partitioning of polyol tracers at a suburban site in Nanjing, east China: increased partitioning to the particle phase, Atmos. Chem. Phys., 21, 12141-12153, 10.5194/acp-21-12141-2021, 2021.
Rastak, N., Pajunoja, A., Acosta Navarro, J. C., Ma, J., Song, M., Partridge, D. G., Kirkevåg, A., Leong, Y., Hu, W. W., Taylor, N. F., Lambe, A., Cerully, K., Bougiatioti, A., Liu, P., Krejci, R., Petäjä, T., Percival, C., Davidovits, P., Worsnop, D. R., Ekman, A. M. L., Nenes, A., Martin, S., Jimenez, J. L., Collins, D. R., Topping, D. O., Bertram, A. K., Zuend, A., Virtanen, A., and Riipinen, I.: Microphysical explanation of the RH-dependent water affinity of biogenic organic aerosol and its importance for climate, Geophysical Research Letters, 44, 5167-5177, 10.1002/2017GL073056, 2017.
Song, M., Marcolli, C., Krieger, U. K., Zuend, A., and Peter, T.: Liquid-liquid phase separation in aerosol particles: Dependence on O:C, organic functionalities, and compositional complexity, Geophysical Research Letters, 39, L19801, 10.1029/2012GL052807, 2012.
Thompson, S. L., Yatavelli, R. L. N., Stark, H., Kimmel, J. R., Krechmer, J. E., Day, D. A., Hu, W., Isaacman-VanWertz, G., Yee, L., Goldstein, A. H., Khan, M. A. H., Holzinger, R., Kreisberg, N., Lopez-Hilfiker, F. D., Mohr, C., Thornton, J. A., Jayne, J. T., Canagaratna, M., Worsnop, D. R., and Jimenez, J. L.: Field intercomparison of the gas/particle partitioning of oxygenated organics during the Southern Oxidant and Aerosol Study (SOAS) in 2013, Aerosol Science and Technology, 51, 30-56, 10.1080/02786826.2016.1254719, 2017.
Topping, D., Connolly, P., and McFiggans, G.: Cloud droplet number enhanced by co-condensation of organic vapours, Nature Geoscience, 6, 443-446, 10.1038/ngeo1809, 2013.
Topping, D. O., Barley, M. H., and McFiggans, G.: The sensitivity of Secondary Organic Aerosol component partitioning to the predictions of component properties – Part 2: Determination of particle hygroscopicity and its dependence on "apparent" volatility, Atmos. Chem. Phys., 11, 7767-7779, 10.5194/acp-11-7767-2011, 2011.
Topping, D. O., and McFiggans, G.: Tight coupling of particle size, number and composition in atmospheric cloud droplet activation, Atmos. Chem. Phys., 12, 3253-3260, 10.5194/acp-12-3253-2012, 2012.
Shulman, M. L., Charlson, R. J., Davis, E. J, The effects of atmospheric organics on aqueous droplet evaporation, Journal of Aerosol Science 28 (5): 737-52,10.1016/S0021-8502(96)00469-7, 1997.
Taflin, D. C., Zhang, S. H. , Allen, T., Davis E. J., Measurement of Droplet Interfacial Phenomena by Light-Scattering Techniques, AIChE Journal 34 (8): 1310-20, 10.1002/aic.690340809, 1988.
Vlasenko, S. S., Su, H., Pöschl, U., Andreae, M. O., and Mikhailov, E. F.: Tandem configuration of differential mobility and centrifugal particle mass analysers for investigating aerosol hygroscopic properties, Atmos. Meas. Tech., 10, 1269-1280, 10.5194/amt-10-1269-2017, 2017.
Wang, J., Doussin, J. F., Perrier, S., Perraudin, E., Katrib, Y., Pangui, E., and Picquet-Varrault, B.: Design of a new multi-phase experimental simulation chamber for atmospheric photosmog, aerosol and cloud chemistry research, Atmos. Meas. Tech., 4, 2465-2494, 10.5194/amt-4-2465-2011, 2011.
Wang, Y., Luo, B., Kleinheins, J., Chen, G. I., Heikkinen, L., and Marcolli, C.: Cloud droplet number enhancement from co-condensing NH3, HNO3, and organic vapours: sensitivity study, EGUsphere, 2025, 1-29, 10.5194/egusphere-2025-4319, 2025.
Wiedensohler, A., Birmili, W., Nowak, A., Sonntag, A., Weinhold, K., Merkel, M., Wehner, B., Tuch, T., Pfeifer, S., Fiebig, M., Fjäraa, A. M., Asmi, E., Sellegri, K., Depuy, R., Venzac, H., Villani, P., Laj, P., Aalto, P.,

https://doi.org/10.5194/ar-2026-14
Preprint. Discussion started: 5 May 2026
© Author(s) 2026. CC BY 4.0 License.

Ogren, J. A., Swietlicki, E., Williams, P., Roldin, P., Quincey, P., Hüglin, C., Fierz-Schmidhauser, R., Gysel, M., Weingartner, E., Riccobono, F., Santos, S., Grüning, C., Faloon, K., Beddows, D., Harrison, R., Monahan, C., Jennings, S. G., O'Dowd, C. D., Marinoni, A., Horn, H. G., Keck, L., Jiang, J., Scheckman, J., McMurry, P. H., Deng, Z., Zhao, C. S., Moerman, M., Henzing, B., de Leeuw, G., Löschau, G., and Bastian, S.: Mobility particle size spectrometers: harmonization of technical standards and data structure to facilitate high quality long-term observations of atmospheric particle number size distributions, Atmos. Meas. Tech., 5, 657-685, 10.5194/amt-5-657-2012, 2012.

Winklmayr, W., Reischl, G. P., Lindner, A. O., and Berner, A.: A new electromobility spectrometer for the measurement of aerosol size distributions in the size range from 1 to 1000 nm, Journal of Aerosol Science, 22, 289-296, 10.1016/S0021-8502(05)80007-2, 1991.

Wu, J., Brun, N., González-Sánchez, J. M., R'Mili, B., Temime Roussel, B., Ravier, S., Clément, J. L., and Monod, A.: Substantial organic impurities at the surface of synthetic ammonium sulfate particles, Atmos. Meas. Tech., 15, 3859-3874, 10.5194/amt-15-3859-2022, 2022.

Yazdani, A., Takahama, S., Kodros, J. K., Paglione, M., Masiol, M., Squizzato, S., Florou, K., Kaltsonoudis, C., Jorga, S. D., Pandis, S. N., and Nenes, A.: Chemical evolution of primary and secondary biomass burning aerosols during daytime and nighttime, Atmos. Chem. Phys., 23, 7461-7477, 10.5194/acp-23-7461-2023, 2023.

Zardini, A. A., Sjogren, S., Marcolli, C., Krieger, U. K., Gysel, M., Weingartner, E., Baltensperger, U., and Peter, T.: A combined particle trap/HTDMA hygroscopicity study of mixed inorganic/organic aerosol particles, Atmos. Chem. Phys., 8, 5589-5601, 10.5194/acp-8-5589-2008, 2008.

Zhang, C., Lu, M., Ma, N., Yang, Y., Wang, Y., Größ, J., Fan, Z., Wang, M., and Wiedensohler, A.: Hygroscopicity of aerosol particles composed of surfactant SDS and its internal mixture with ammonium sulfate at relative humidities up to 99.9%, Atmospheric Environment, 298, 119625, 10.1016/j.atmosenv.2023.119625, 2023.

Zhang, J., Zuend, A., Top, J., Surdu, M., Ei Haddad, I., Slowik, J. G., Prevot, A. S. H., and Bell, D. M.: Estimation of the Volatility and Apparent Activity Coefficient of Levoglucosan in Wood-Burning Organic Aerosols, Environmental Science & Technology Letters, 11, 1214-1219, 10.1021/acs.estlett.4c00608, 2024.